Electronic Supplementary Material (ESI) for Nanoscale.
This journal is © The Royal Society of Chemistry 2021

Supporting Information

Electrical energy generation by squeezing ions in diffusion layer of electrical double layer

Xiaoshuang Zhou [a], Xin Chen [a], Hao Zhu [a], Xu Dong [a], Guanggui Cheng [b], Zhongqiang Zhang [b], Xinghao Hu*[, b], Ningyi Yuan*[, a], Jianning Ding*[, a, b]
a Jiangsu Collaborative Innovation Center for Photovoltaic Science and Engineering; Jiangsu Province Cultivation base for State Key Laboratory of Photovoltaic Science and Technology, Changzhou University, Changzhou 213164, P. R. China
b Institute of Intelligent Flexible Mechatronics, Jiangsu University, Zhenjiang, 212013, P. R. China

* Email: dingjn@ujs.edu.cn, nyyuan@cczu.edu.cn, huxh@ujs.edu.cn

Experimental supplement for comparing

Fabrication of rGO / PEDOT aerogel

A: Graphene oxide dispersion (5mg mL^{-1}) was first mixed with ethane diamine by stirring and ultrasonic dispersion for 5min. B: 24mg 4-(3-butyl-1-imidazolio-1-butanesulfonic acid triflate BIBAST (45.5%), 0.275mg 4,4'-diazido-2.-2'-stilbenedisulfonic acid disodium salt N_3-SADS，3.05mg $CuCl_2$ was added into 5 mL PEDOT: PSS(1.5wt%) under a quick stir, then 5ml acetonitrile was added and stirred for 1min. Successively, A: B was evenly mixed in the different ratio to get resulting mixture. The resulting mixture was then sealed in a glass vial and heated for 9h at 120 ^oC for synthesis of partially reduced graphene hydrogel. Then, the obtained hydrogel was immersed in 5% (volume ratio) ethanol water solution for 6h. Thirdly, the wet hydrogel was freeze-dried in dryer for 72h (pre-freeze at -20℃ for 4h). Finally, GO aerogel was further reduced in tube oven at 180 ^oC for 2h.

Fabrication of rGO / CNT aerogel

Graphene oxide dispersion (5mg mL^{-1}) and 2.5mg/mL CNTs dispersion was first mixed with ethane diamine by stirring and ultrasonic dispersion for 5min. After that, we poured the mixed solution into a quartz bottle, which was put into the PTFE bottles in a stainless-steel autoclave, the hydrogel was prepared successfully with a constant temperature of 120°C for 6 hours. The obtained hydrogel was washed several times with an 8% hydroalcoholic solution, and soaked for a whole day. After that, we took out the graphene hydrogel and made it freeze-dry for 48 hours to obtain rGO / CNT aerogel.

We fabricated four graphene-based aerogels mainly, they all works for harvesting energy by the compressing experiment. (output voltage: rGO~160mV, rGO-MXene ~265mV, rGO-PEDOT~250mV, rGO-CNTs~215mV)

Calculation of power conversion efficiency

The power conversion efficiency was defined as the ratio of mechanical energy into electric energy. The mechanical energy was collected from mechanical testing system (QT-62035, Qian tong Instrument Equipment Co. Ltd). The stress strain curve of the aerogel device when compressed to 20% strain in 0.5M NaCl electrolyte is shown in Fig. S4. The mechanical lost between compression and release was calculated from it (33.1J/kg, the value was calculated by integrating the area of the stress-strain curve, and then normalized to aerogel mass). The total electric output work of the device was calculated by $W = \int_{to}^{t1} Pdt$. Therefore, the electrical energy generated per cycle was about 14.3 J/kg (the value was calculated by integrating the area of time-power curve, and then normalized to aerogel mass), the corresponding conversion efficiency of the aerogel harvester device was obtained as 43.2% (The hysteresis was not taken into account) ($e \approx 14.3/33.1 \approx 43.2\%$). The mechanical lost here represented the mechanical input. We used the mechanical sensors to test the changed displacement and force under the aerogel. The applied force and the recovered force reflected the whole process of force for the aerogel materials. W=∫F*s was used to calculated the work during the process, then normalized to aerogel mass, which has been added. Meanwhile, this calculation is referred to the science's work (Figure S18 S19 and related descriptions) (Kim, Shi Hyeong, et al. "Harvesting electrical energy from carbon nanotube yarn twist." Science 357.6353 (2017): 773-778.)

Poiseuille model with boundary slip

Here we add the acceleration of a_x on the fluid in x direction, then the confined fluid can be described by a parabolic solution of the Navier-Stokes (N-S) equation. For the Poiseuille fluids confined in microchannels with the channel width of H (from $-\frac{H}{2}$ to $\frac{H}{2}$ in z direction), the N-S equation can be written by

$$\frac{\partial^2 v_x}{\partial z^2} = -\frac{\rho a_x}{\eta}, \tag{1}$$

where η is the shear viscosity, v_x is the flow velocity while x is the flow direction, and z is the direction across the channel ρ is the density of the confined fluid. Then, we integrate Eq. (1), and substitute the center symmetry condition $\left.\frac{\partial v_x}{\partial z}\right|_{z=0} = 0$ and the boundary slip condition $v_x|_{z=\pm\frac{H}{2}} = v_s$ where v_s is the slip velocity at the two fluid-solid boundaries. Then, the velocity profile of this Poiseuille flow can be written as

$$v_x = \frac{\rho a_x}{2\eta}\left(\frac{H^2}{4} - z^2\right) + v_s. \tag{2}$$

Correspondingly, the shear stress within the fluid is $\tau_{xz} = \eta\dot{\gamma}$, where the shear rate $\dot{\gamma} = \frac{dv_x}{dz}$. Then, the shear stress can be described as

$$\tau_{xz} = -\rho a_{x_Z}. \tag{3}$$

Thus, the maximum shear stress appears at the boundaries, i.e.,

$$\tau_{xz}|_{z=\pm\frac{H}{2}} = -\rho a_x\left(\pm\frac{H}{2}\right). \tag{4}$$

Calculation of specific capacitance

C_m was calculated by using the CV method. The formula is following：

$$C_m = Q/2Vm = \frac{\int_{V2}^{V1} i\ (V)\ dV}{2Vvm}$$

Where *m, Q, V, v and i(V)* are the mass of aerogel material, the total charge, voltage window, scanning rate and current, respectively.

Calculation details

The mass used for specific power density and energy density was just the mass of the aerogel.

The power calculation:

$P = \Delta U^2/R$

Where ΔU is peak-to -peak voltage under the loading resistance, R is the loading resistance in the circuit.

Error bars

The error bars were calculated from the standard deviation at different measurement cycle (3-5 cycle).

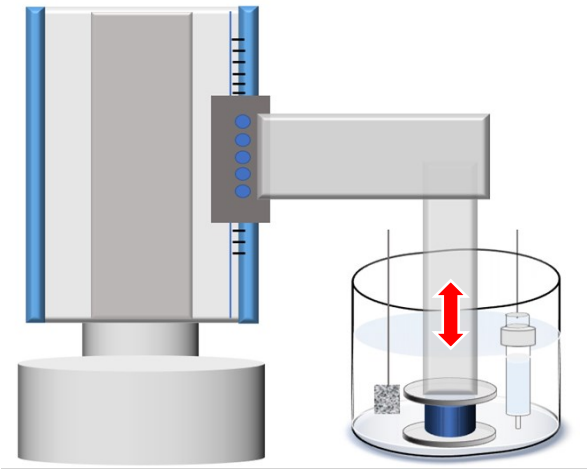

Figure S1. The illustration of measurement system for Compression graphene-based harvester including Reciprocating extrusion equipment, graphene-based electrode and counter and reference electrodes in an electrochemical bath.

(a)

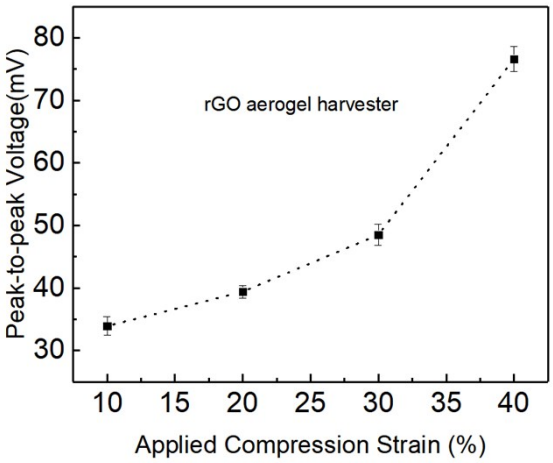

(b)

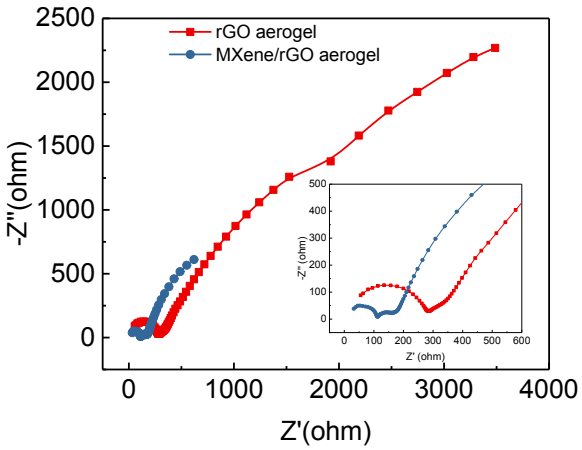

(c)

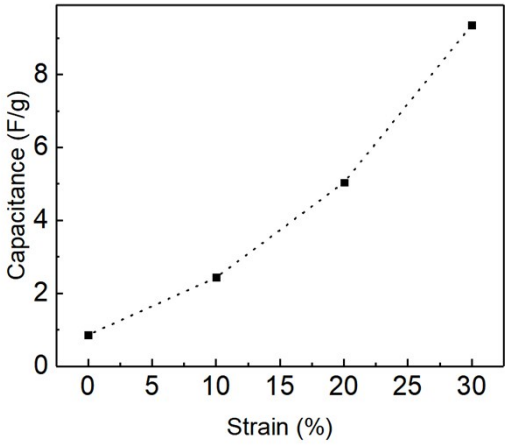

Figure S3. (a) The open-circuit voltage (OCV) versus applied strain for a rGO aerogel harvester in 0.1M TEA·BF_4/PC electrolyte. (Error bars: standard deviation) (b) EIS result taken from100 kHz to 10 mHz, with an insert displaying the enlarged plot at high frequency region, in 0.1M TEA·BF_4/PC electrolyte. (c) The fitted specific capacitance from EIS versus applied strain for a MXene/rGO aerogel in the electrolyte.

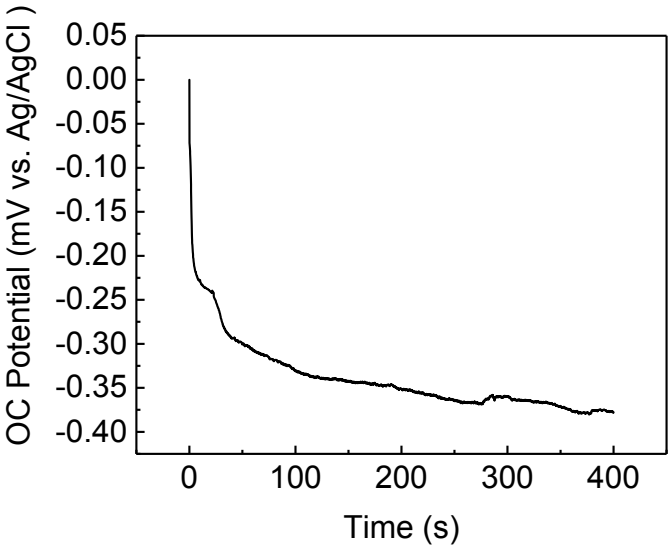

Figure S3. The initial open circuit potential as function of time for a MXene/rGO aerogel harvester in 0.5M NaCl electrolyte.

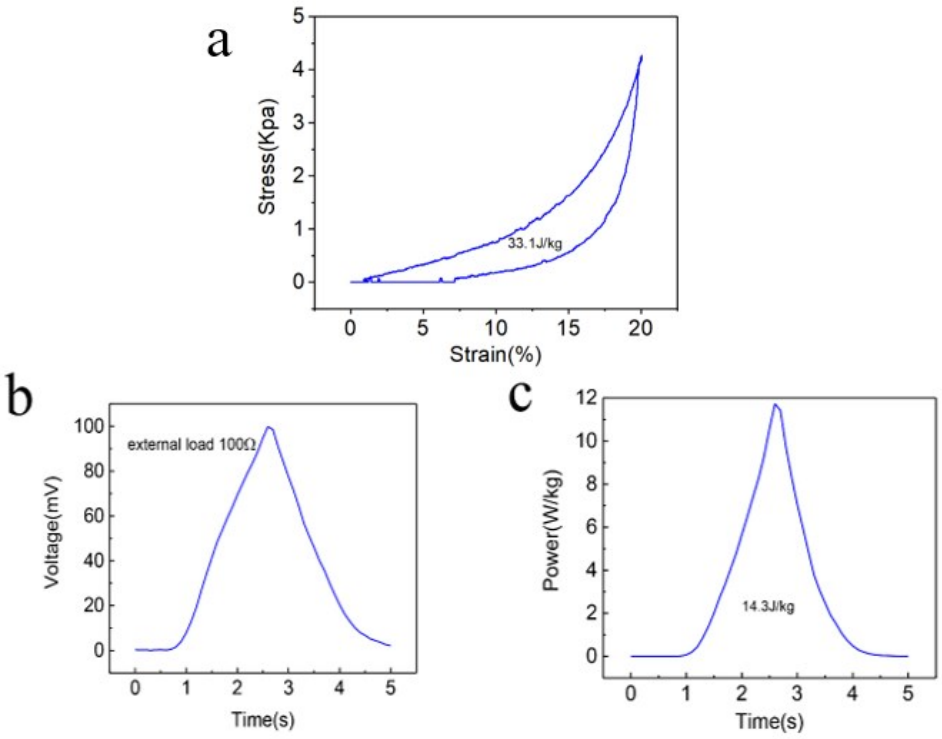

Figure S4. Efficiency of MXene/rGO aerogel harvester under 20% applied compression strain in 0.5M NaCl. **(a)** The stress strain curve of the aerogel harvester. **(b)** The voltage generated on a 100-ohm load during the compressing (one cycle compression).

Considering the hysteresis in figureS4a, we assured that the hysteresis is main due to the aerogel itself, because we find that the hysteresis exists among most aerogel even squeezed in air [21-24]. Also, the aerogel squeeze in liquid maybe enhance the hysteresis due to electrolyte adhesion in the channel network.

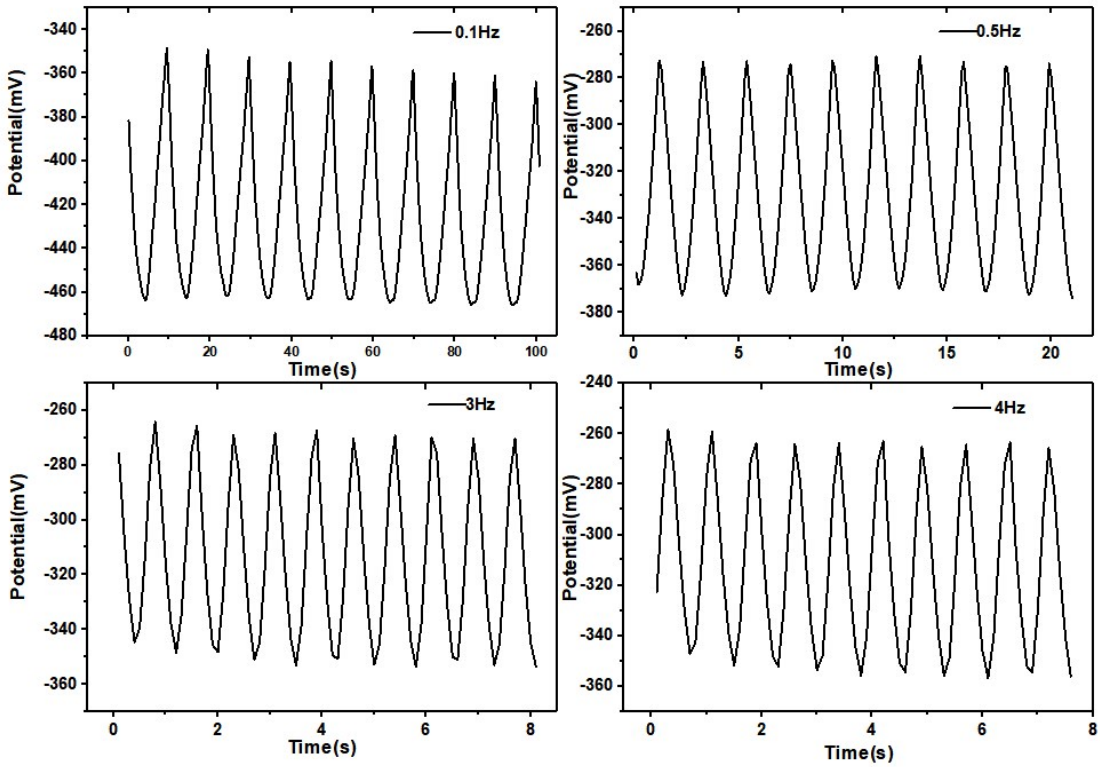

Figure S5. The open-circuit voltage (OCV) at different compressive frequencies for a MXene/rGO aerogel harvester in 0.1M TEA·BF_4/PC electrolyte.

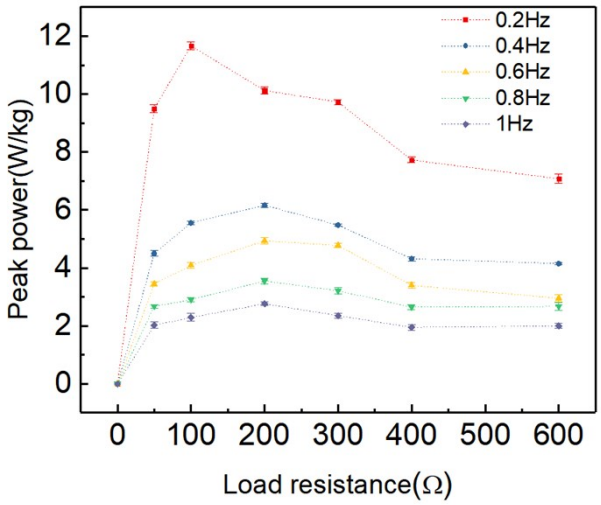

Figure S6. Load resistance dependence of peak power for different compressing frequencies under 20% compression strain of an aerogel harvester in 0.5M NaCl aqueous electrolyte. (Error bars: standard deviation)

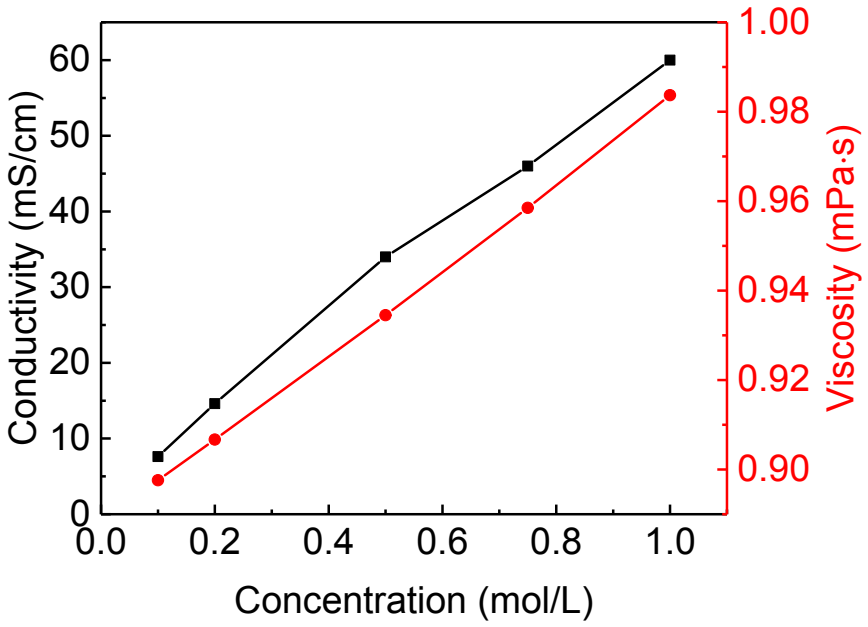

Figure S7. The conductivity and viscosity for different concentrations of NaCl electrolyte.

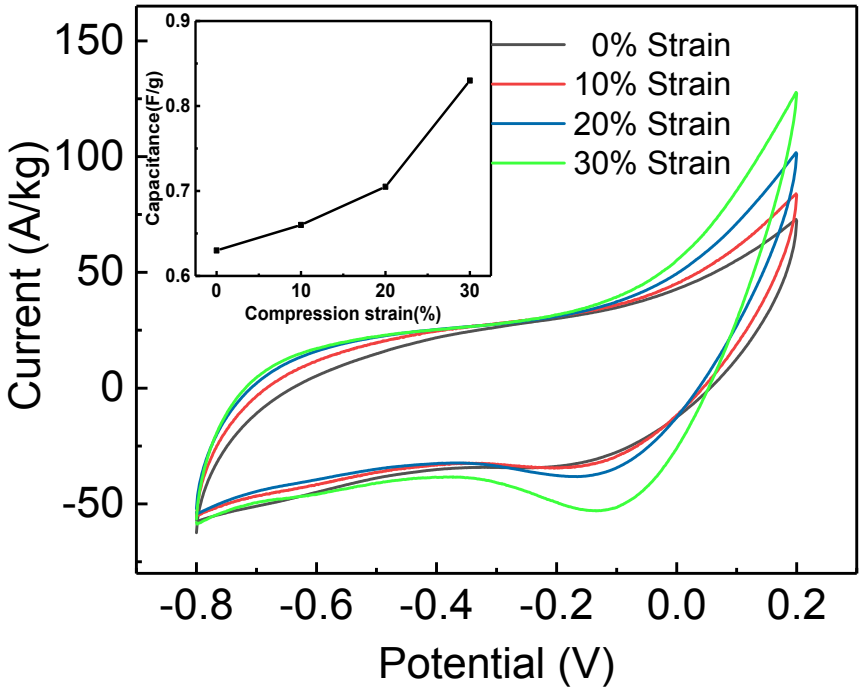

Figure S8. CV curves of different compression strain for the harvester in 0.5M NaCl electrolyte.

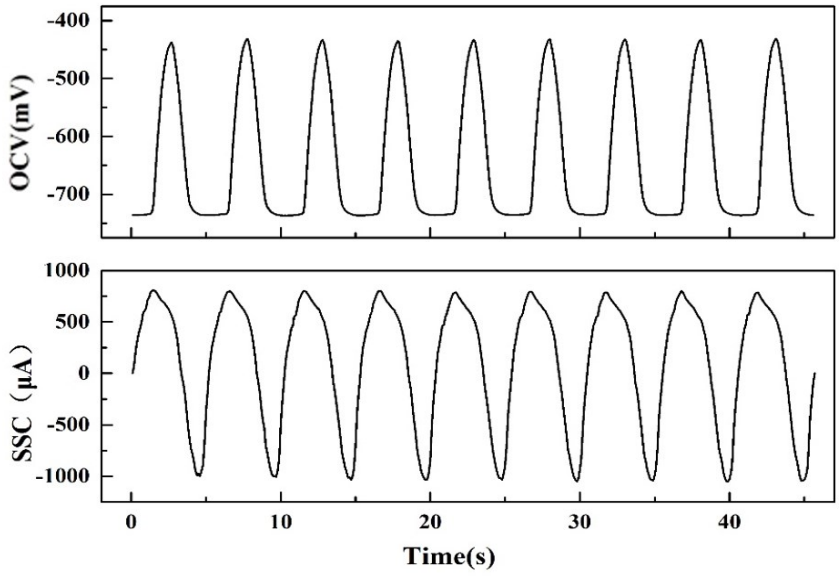

Figure S9. Applied pressure strain (30%) and resulting change in open-circuit voltage (OCV) and short circuit current (SSC) for an aerogel harvester in 0.5M NaCl aqueous electrolyte at 0.2Hz.

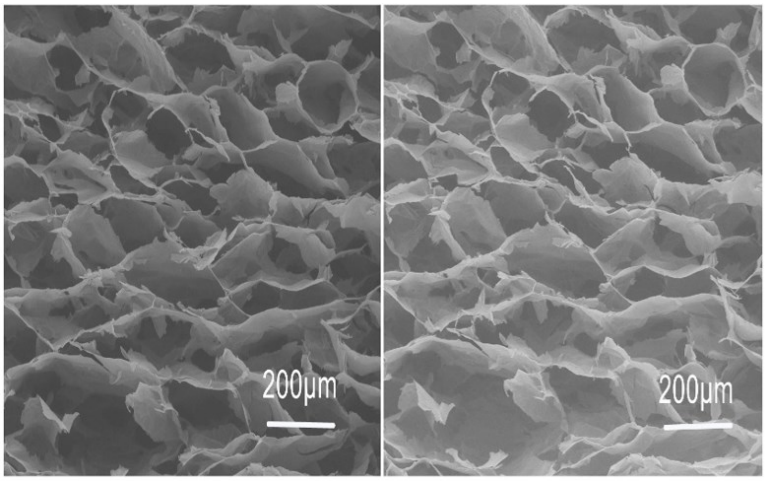

Figure S10. The SEM sectional images of aerogel before and after compression

As is shown in Figure S9, the change of macroscopic structure was visible, after releasing the stress, the MX/rGO aerogel nearly recovered its original shape.

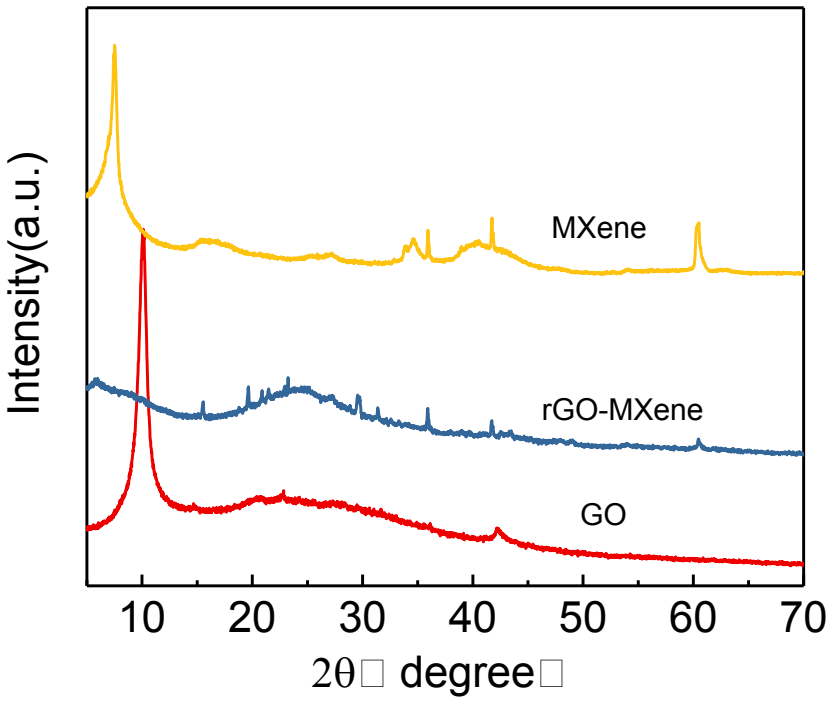

Figure S11 XRD patterns of MXene and rGO-MXene and GO powder

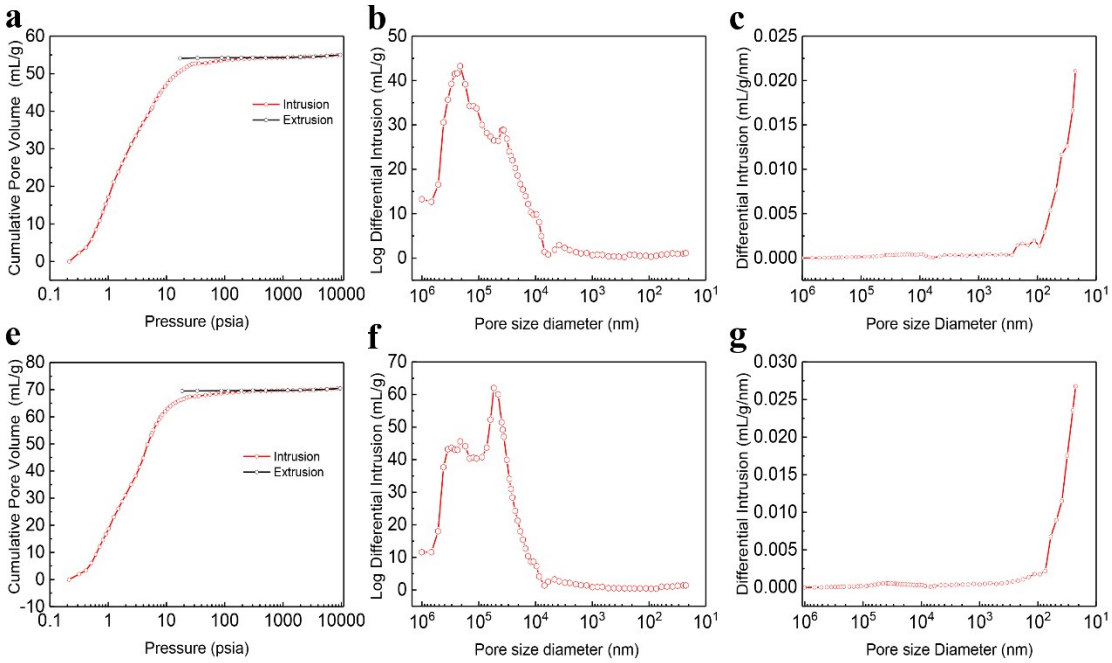

Figure S12 The Porosity and pore size distribution measurement curves for composite aerogels. (a) (b) (c) pure rGO aerogel (e) (f) (g) rGO-MXene aerogel.

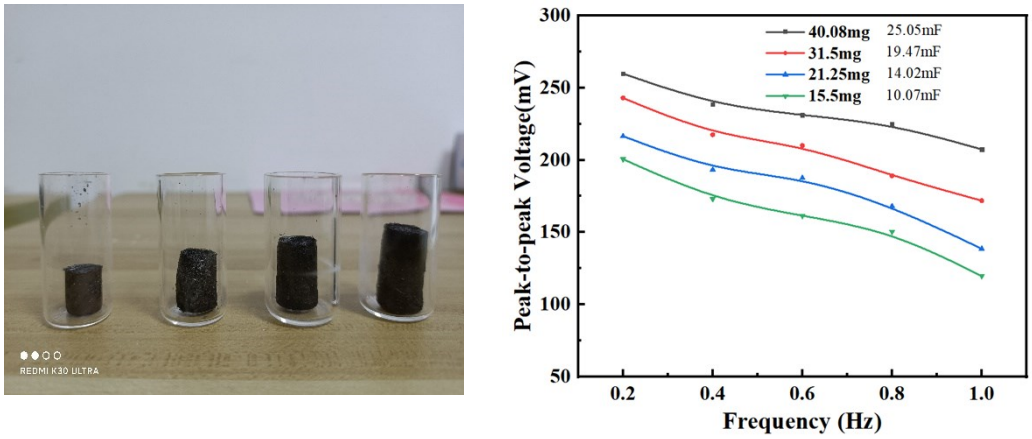

Figure S13. The photos of aerogels with different wights and the output performance and capacitance (calculated from CV curves) of them.

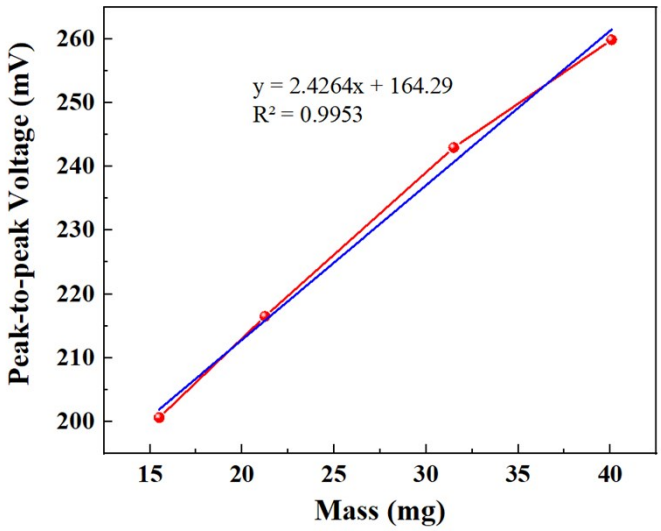

Figure S14. The dependence of mass with output voltage.

Figure S15. Pump oil absorption and combustion experiment

According to our experiment, the aerogel can absorb ~100 times of self-weight of pump oil (0.04g adsorb 4g).

TableS1. Aerogel harvester performance compared with that other solid-state energy harvesters recently.

Category	Dimension	Peak OCV	SCC	Peak power	Efficiency	Ref.
Graphene/MXene aerogel	3D	300mV	~1000μA	11.7W/kg	43.2%	**This work**
CNT yarn	1D	~180mV	~80μA	250W/kg	1.05%	[1]
GO film	2D	~150mV	/	/	/	[2]
CNT fiber	1D	165mV	22μA	39.5 mWg^{-1}	23.3%	[3]
GO flim	2D	0.7V	/	0.27 W m^{-2}	/	[4]
ZnO flim	2D	~0.4 V	~20 nA	/	/	[5]
Carbon film	2D	0.79 ± 0.05 V	/	150 W/m^2	/	[6]
Aramid nanofibers and BN flim	2D	60mV	1.8μA	0.6 W m^{-2}	/	[7]
Graphene flim	2D	0.1V	10nA	/	/	[8]
rGO /paper flim	2D	~270mV	/	53mW/cm^2	/	[9]
Graphene foam	3D	~200μV	10μA	/	/	[10]
Wood channels	3D	300mV	10μA	/	/	[11]

Table S2. Summary of electric energy harvesters based on aerogel

Materials	Mechanism	Peak OCV	SCC	Peak power	Efficiency	Ref.
Graphene/Mxene	electrochemistry	~300mV	~1000μA	11.7W/kg	43.2%	This work
Graphene foam	electrochemistry	~200μV	10μA	\	\	[10]
PDMS/ZnO/ 3D Graphene foam	Piezoelectric / Triboelectric	120V	51μA/cm^2	6.22 mW/cm	\	[12]
PAAm-LiCl-resin foam	Triboelectric	~65V	45mA/m^3	10.98 W/m^3	\	[13]
Polyurethane aerogel	Triboelectric	~105.6V	20.3μA	0.56mW/cm^3	\	[14]
Cellulose-based aerogels	Triboelectric	~200V	0.5μA	\	\	[15]
Silk/Silk Composite Aerogel	Triboelectric	52.8V	5.2μA	0.37 W/m^2		[16]
PDMS foam	Piezoelectric	100mV	~1nA	5μW/m^2	/	[17]
Cellulose/$BaTiO_3$ aerogel	Piezoelectric	15.5V	3μA	11.8μW	\	[18]
Carbon nanotube aerogel	Electrochemical thermal	22mV	\	6.6W/m ^{2}	3.95%	[19]
Carbon nanofiber aerogels	Thermoelectric	80mV	9mA (750s)	1.2W/m^2	96.2%	[20]
graphene–carbon nanotube aerogels	Electrochemical thermal	120mV	0.8A/g	65 W/kg	~3.5	[21]

Compared to other aerogel harvesters, there are relatively few aerogels that involve electrochemistry. Most are piezoelectric, triboelectric, electrothermal or electrochemical thermal. As for electrochemistry, Huang et al. synthesized a graphene foam on a porous nickel platform to induce electricity of ~25 μA at biased voltage of

80 μV and with a fluid velocity of 80 cm s^{-1},[10] which is based on flow-induced potentials. For piezoelectric or triboelectric aerogel harvesters, they can generate dozens or even hundreds of voltages, but the current is usually a few microamps or less. [12-18] Meanwhile, the aerogel harvesters based on electrochemical thermal can generate relative high voltage and current, but the device performance relative to cost has so far limited application for waste heat recovery. [19,20] Recently, thermoelectric materials combined with aerogel materials was also investigated, Niu et al. fabricated an efficient thermo- and sunlight-driven energy harvester by the combination of organic phase change materials (OPCM) with carbon nanofiber aerogels (CNFAs). The maximum voltages generated by the energy harvesting system are 55 and 80 mV corresponding to the thermo- and sunlight driven energy harvesting process, respectively, with a maximum power density of 0.50 W/m^2 and 1.20 W/m^2 in each process. However, the whole process needs dozens of minutes.[21]

Table S3. Comparisons of capacitive energy generators

Architecture	Peak OCV	SCC	Peak power density	Efficiency	Ref.
CNT yarns in salt solution	~180mV	~80μA	250W/kg (30Hz)	1.05%	[1]
CNT fiber in flow solution	~165mV	~22μA	39.5 mWg^{-1}	23.3%	[3]
Li-alloyed Si electrodes	22.5mV	14.5μA	0.53μW /cm^2	0.62%	[25]
PTFE on ITO	14 droplets 30Hz 8V	/	0.3μW /cm^2 (1ml of water)		[26]
Silica channel	~5V		240pW (490 nm high)	3.2%	[27]

Table S4. The data for porosity and pore size distribution measurement

Sample	Mass (g)	Porosity (%)	Total pore volume (ml/g)	Total pore area (m^2/g)	Average pore volume (ml/g)	Average pore area (m^2/g)
rGO aerogel	0.0039	91	54.9871	65.1749	33.4341	1.3695
rGO-MXene aerogel	0.0044	95	70.4784	79.2701	42.2296	1.9162

As can be seen from the figures and table, it finds that the addition of MXene make the aerogel have a bigger porosity, and for two kinds of aerogel are mainly dominated by the macropores.

Caption for Supporting Movie

Movie S1. An aerogel harvester was compressed at 1Hz under the motor device.

Movie S2 A LED light was lightened by an aerogel harvester and a boost converter circuit (for increasing the output voltage)

References

[1] S.H. Kim, C.S. Haines, N. Li, K.J. Kim, T.J. Mun, C. Choi, J. Di, Y.J. Oh, J.P. Oviedo, J. Bykova, Harvesting electrical energy from carbon nanotube yarn twist, *Science.* **2017**, 357, 773-778.

[2] L. Huang, J. Pei, H. Jiang, C. Li, X. Hu, Electricity generation across graphene oxide membranes, *Materials Research Bulletin*. **2018**, 96-100.

[3] Y. Xu, P. Chen, J. Zhang, S. Xie, F. Wan, J. Deng, X. Cheng, Y. Hu, M. Liao, B. Wang, A One-Dimensional Fluidic Nanogenerator with a High Power Conversion Efficiency, *Angewandte Chemie International Edition*. **2017**, 56, 12940-12945.

[4] Y. Liang, F. Zhao, Z. Cheng, Y. Deng, Y. Xiao, H. Cheng, P. Zhang, Y. Huang, H. Shao, L. Qu, Electric power generation via asymmetric moisturizing of graphene oxide for flexible, printable and portable electronics, Energy & Environmental Science. **2018**, 11, 1730-1735.

[5] S.G. Yoon, Y. Yang, J. Yoo, H. Jin, W.H. Lee, J. Park, Y.S. Kim, Natural Evaporation-Driven Ionovoltaic Electricity Generation, *ACS Applied Electronic Materials*. **2019,** 1(9), 1746-1751.

[6] G. Zhang, Y. Xu, Z. Duan, W. Yu, C. Liu, W. Yao, Conversion of low-grade heat via thermal-evaporation-induced electricity generation on nanostructured carbon films, *Applied Thermal Engineering*. **2020**, 166 114623.

[7] C. Chen, D. Liu, L. He, S. Qin, J. Wang, J.M. Razal, N.A. Kotov, W. Lei, Bio-inspired nanocomposite membranes for osmotic energy harvesting, *Joule*. **2020**, 4, 247-261.

[8] J. Yin, Z. Zhang, X. Li, J. Yu, J. Zhou, Y. Chen, W. Guo, Waving potential in graphene, *Nature Communications*. **2014**, 5(1), 1-6.

[9] R.K. Arun, P. Singh, G. Biswas, N. Chanda, S. Chakraborty, Energy generation from water flow over a reduced graphene oxide surface in a paper–pencil device, *Lab on a Chip.* **2016**, 16, 3589-3596.

[10] X. Zhou, W. Zhang, C. Zhang, Y. Tan, J. Guo, Z. Sun, X. Deng, Harvesting Electricity from Water Evaporation through Micro-Channels of Natural Wood, *ACS Applied Materials & Interfaces*. **2020** 12, 11232-11239.

[11] W. Huang, G. Wang, F. Gao, Z. Qiao, G. Wang, L. Tao, M. Chen, F. Yu, H. Yang, L. Sun, Power generation from water flowing through three-dimensional graphene foam, *Nanoscale*. **2014**, 6, 3921-3924.

[12] Y. Qian, and J. Dae. Poly (dimethylsiloxane)/ZnO nanoflakes/three-dimensional graphene heterostructures for high-performance flexible energy harvesters with simultaneous piezoelectric and triboelectric generation. *ACS Applied Materials & Interfaces*. **2018,** 10(32), 32281-32288.

[13] B. Chen,W. Tang, T. Jiang, L. Zhu, X. Chen, C. He, L. Xu, H. Guo, P. Lin, D. Li, J. Shao, Z. Wang, Three-Dimensional Ultraflexible Triboelectric Nanogenerator Made by 3D Printing. *Nano Energy*. **2018**, 45, 380-389.

[14] Z. Saadatnia , S. Mosanenzadeh, T. Li, E. Esmailzadeh, H. Naguib, Polyurethane aerogel-based triboelectric nanogenerator for high performance energy harvesting and biomechanical sensing. *Nano Energy*. **2019**, 65, 104019.

[15] L. Zhang, Y. Liao, Y. Wang, S. Zhang, W. Yang, X. Pan, Z. Wang, Cellulose II Aerogel-Based Triboelectric Nanogenerator. *Advanced Functional Materials*.2020, 2001763.
[16] H.Mi, H. Li, X. Jing, P. He, P. Feng, X. Tao, C. Shen, Silk and Silk Composite Aerogel Based Biocompatible Triboelectric Nanogenerators for Efficient Energy Harvesting. *Industrial & Engineering Chemistry Research.*2020.
[17] C. Petroff, T. Bina, G. Hutchison, Highly Tunable Molecularly Doped Flexible Poly (dimethylsiloxane) Foam Piezoelectric Energy Harvesters. *ACS Applied Energy Materials*. **2019**, 2(9), 6484-6489.
[18] K. Shi, X. Huang, B. Sun, Z. Wu, J. He, P. Jiang, Cellulose/BaTiO3 aerogel paper based flexible piezoelectric nanogenerators and the electric coupling with triboelectricity. *Nano Energy*. **2019**, 57, 450-458.
[19] H. Im, T. Kim, H. Song, J. Choi, J. Park, R. Ovalle-Robles, Y. Kim, High-efficiency electrochemical thermal energy harvester using carbon nanotube aerogel sheet electrodes. *Nature Communications*. **2016**, 7(1), 1-9.
[20] S. Gupta, R. Meek, Highly efficient thermo-electrochemical energy harvesting from graphene–carbon nanotube 'hybrid'aerogels. *Applied Physics A*.**2020**, 126(9), 1-12.
[21] Z. Niu, W. Yuan, Highly efficient thermo-and sunlight-driven energy storage for thermo-electric energy harvesting using sustainable nanocellulose-derived carbon aerogels embedded phase change materials. *ACS Sustainable Chemistry & Engineering*. **2019**, 7(20), 17523-17534.
[22] Zhuo H, Hu Y, Tong X, Chen Z, Zhong L, Lai H, Liu L, Jing S, Liu Q, Liu C, Peng X. A supercompressible, elastic, and bendable carbon aerogel with ultrasensitive detection limits for compression strain, pressure, and bending angle, *Advanced Materials*. **2018**, 30:1706705.
[23] Ma Y, Yue Y, Zhang H, Cheng F, Zhao W, Rao J, Luo S, Wang J, Jiang X, Liu Z, Liu N. 3D synergistical MXene/reduced graphene oxide aerogel for a piezoresistive sensor. *ACS Nano*. **2018**, 12:3209-16.
[24] Yue Y, Liu N, Ma Y, Wang S, Liu W, Luo C, Zhang H, Cheng F, Rao J, Hu X, Su J. Highly self-healable 3D microsupercapacitor with MXene–graphene composite aerogel. *ACS Nano*. **2018**, 12:4224-32.
[25] S. Kim, S. Choi, K. Zhao, H. Yang, G. Gobbi, S. Zhang, J. Li, Electrochemically driven mechanical energy harvesting. *Nature Communications*.**2016**, 7(1), 1-7.
[26] J. Moon, J. Jeong, D. Lee, H. Pak, Electrical power generation by mechanically modulating electrical double layers. *Nature Communications.* **2013**, 4(1), 1-6.
[27] F. van der Heyden, D. Bonthuis, D. Stein, C. Meyer, C. Dekker, Power generation by pressure-driven transport of ions in nanofluidic channels. *Nano Letters*.**2007**, 7(4), 1022-1025.